ACS OMEGA

Open Access

http://pubs.acs.org/journal/acsodf

Article

Sustainable Green Route for Activated Carbon Synthesis from Biomass Waste for High-Performance Supercapacitors

Maasoomeh Jafari and Gerardine G. Botte*

Cite This: *ACS Omega* 2024, 9, 13134−13147

Read Online

ACCESS | Metrics & More | Article Recommendations | Supporting Information

ABSTRACT: Supercapacitors are high-power energy storage devices due to their charge storage capability and long cyclic stability. These devices rely on highly porous materials for electrodes providing a substantial surface area per mass, such as highly porous carbon. Developing high-performance porous carbon from biomass wastes such as waste-activated sludge and spent coffee is a sustainable way to reduce adverse environmental effects, contributing toward a carbon circular economy. In this study, hierarchically porous carbon with a high surface area of 1198 ± 60 m^2 g^{-1} was synthesized through a green route. Sodium acetate was utilized as an environmentally friendly electrolyte. The long-term stability test at a high current density was conducted, providing valuable insights into the viability of sodium acetate as a robust electrolyte in supercapacitor application. The supercapacitor demonstrated an excellent cycle stability of 98.4% after 20,000 cycles at a current density of 10 A g^{-1} in sodium acetate. Further assessment revealed dominant fast surface kinetics. Moreover, a maximum energy density of 15.9 Wh kg^{-1} at 0.2 A g^{-1} was achieved. By utilizing highly porous carbon in conjunction with a water-based binder, a substantial improvement of 76% in capacity with respect to a nonaqueous-based binder was demonstrated.

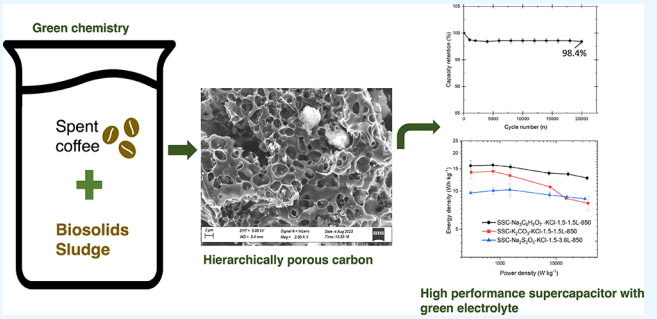

1. INTRODUCTION

Supercapacitors are characterized by high power density, fast charging/discharging rates, and remarkable long-term stability (>10,000 cycles).[1] Energy storage and delivery technologies such as supercapacitors possess the capability to store and deliver energy at an extremely fast rate, providing a high current over a short period. Hence, they are applicable in electric vehicles (EVs), uninterruptible power supplies (UPS), and hybrid buses.[2] The most common type of supercapacitor is an electrochemical double-layer capacitor (EDLC). EDLC supercapacitors store charges through the adsorption and desorption of electrolyte ions at electrodes, in contrast to batteries that depend on electrochemical redox reactions.[3] This distinction has enabled supercapacitors to achieve impressive high power densities, surpassing lithium-ion batteries by an order of magnitude. The electrochemical performance of the supercapacitors is limited by the electrode materials. It is crucial to develop highly porous carbon-based electrode materials featuring a high specific surface area that can be readily accessed to electrolyte ions. Accessibility of the specific surface area depends on the pore size distributions. Pore sizes smaller than 0.5 nm are not accessible to hydroxide ions when aqueous electrolytes are used (e.g., potassium hydroxide) and pore sizes below 1 nm are not accessible to organic electrolytes.[4]

Porous carbons are the key component in many applications including adsorption and energy storage systems such as supercapacitors and lithium batteries.[5] The demand for porous carbon is expected to substantially increase over the next few years. The high-cost petroleum-based active carbon ($4000 per ton) is the commercial material that is currently being used.[6] The operating voltage window and specific capacitance of the commercial supercapacitors are 2.7 V and 100−120 F g^{-1} in organic electrolytes and 1.23 V and 200 F g^{-1} in aqueous electrolytes.[2] Biomass-derived porous carbons are considered the most reliable carbon source due to their low cost, availability, and sustainability. In recent years, the use of activated carbons derived from biomass, especially biowaste, has sparked substantial interest in the energy storage device community.[7−12] This popularity is primarily due to the inexpensiveness, sustainability, and abundance of the raw materials. To date, several biowastes have been utilized to synthesize activated carbon; however, the applications are still restricted due to undesirable pore structures. The synthesis methods play a vital role in controlling the carbonization process and pore size distributions to meet the required criteria

Received: December 2, 2023
Revised: January 22, 2024
Accepted: February 29, 2024
Published: March 8, 2024

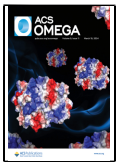

for supercapacitor applications. The ideal porous carbon for supercapacitors should possess several key characteristics including a large specific surface area to accommodate charge storage, hierarchical pores (micro (<2 nm), meso (2−50 nm), and macro (>50 nm)) to facilitate fast ion transport diffusion, and excellent wettability to enhance access of electrolyte ions to the pores.[13] Waste-activated sludge (WAS) and spent coffee (SC) are ideal candidates to convert into porous carbon for energy storage applications due to their high organic content and their functional groups.[14,15] Tremendous amounts of WAS (45 million tons) and SC (15.33 million tons) are generated annually around the world, which will end up mostly in landfills.[16,17] Landfilling these biowastes releases greenhouse gases including 28.644 million tons of carbon dioxide and 21 million tons of methane annually.[18,19] Hence, converting waste to activated carbon for energy storage applications could solve environmental issues related to waste landfilling. The hydrophilic nature of WAS and SC due to their surface functional groups makes the material wettable with aqueous electrolytes and rapid ion diffusion to the pores, which results in obtaining a higher capacity.

Traditional transformation routes of biomass to porous carbon materials involve corrosive chemicals such as hydrogen fluoride (HF), potassium hydroxide (KOH), and zinc chloride ($ZnCl_2$), which also hinder the economic feasibility, environmental friendliness, and scaling of the processes.[20−24] For instance, Li et al. synthesized porous carbon from oily sludge using HF pretreatment, KOH as the activation agent, and hydrochloric acid (HCl) for the washing step, which resulted in producing different hazardous waste streams.[25] Also, utilizing the microwave-assisted process for porous carbon synthesis is not applicable to large scale due to challenges such as the lack of uniform heating, safety concerns (thermal runaway), and energy distribution (limited penetration depth of microwaves).[26] The production process of activated carbon needs to be eco-friendly and easy to scale up. Therefore, it is imperative to use environmentally friendly alternatives for activating chemicals such as sodium thiosulfate, carbonate salts, and molten salts (e.g., potassium chloride and sodium chloride).[27]

Utilization of flammable organic electrolytes (e.g., tetraethylammonium tetrafluoroborate (TEA-BF4) in propylene carbonate or acetonitrile) in EDLCs causes numerous safety issues. In addition, traditional aqueous electrolytes such as sulfuric acid and potassium hydroxide have limited operating potential to 1 V.[25,28] Hence, the supercapacitors made with conventional electrolytes have a low energy density (<10 Wh kg^{-1}).[25] To develop high-energy-density and eco-friendly supercapacitors, it is essential to use a green electrolyte with a wider operating potential window (>1 V), which can maintain capacity for a long operating time (>10,000 cycles) in a coin cell.

In this study, a green, facile, and scalable route of production of activated carbon from WAS and SC waste was developed by using sodium thiosulfate, potassium carbonate, and trisodium citrate as the green activation agents. Notably, no prior studies have explored the synthesis of porous carbon from mixtures of WAS and SC waste using these specified chemicals. The effects of the activation agents with a molten salt aid (e.g., potassium chloride), mixing method, and operating temperature on the physiochemical properties of the activated carbons were evaluated. The electrochemical performance of supercapacitors made with synthesized activated carbon was investigated by incorporating different binding materials into a traditional aqueous electrolyte. It is worth noting that in this study, a green electrolyte (sodium acetate) with a wide operating potential window (∼1.5 V) was used to obtain a high-energy-density supercapacitor. The kinetic and mass transfer processes were examined using cyclic voltammetry with an ultrafast scan rate ranging from 20 to 1000 mV s^{-1} and electrochemical impedance spectroscopy, respectively. To the best of our knowledge, no prior studies have investigated the long-term stability test as well as the kinetic and mass transfer process of a biomass-based supercapacitor using a sodium acetate electrolyte.

2. EXPERIMENTAL SECTION

2.1. Materials. Sludge samples were taken from the Lubbock, Texas, wastewater treatment plant after centrifugal drying, the last step in the process before landfill disposal. Spent coffee samples were obtained from premium roast McCafé after filter brewing. Both spent coffee and sludge samples were dried in an oven (Across International) at 100 °C overnight (24 h). Sodium thiosulfate pentahydrate ($Na_2S_2O_3·5H_2O$, 99.7%, Fisher Scientific), potassium carbonate anhydrous (K_2CO_3, ACS grade, >99%, Sigma-Aldrich,), potassium chloride (KCl, free-flowing, purity of >99%, Redi-Dri, ACS reagent, Sigma-Aldrich), and trisodium citrate dihydrate ($Na_3C_6H_5O_7·2H_2O$, 99%, Alfa Aesar) were utilized as the activation agent. Potassium hydroxide (KOH, 85%, Fisher Scientific) and sodium acetate anhydrous (CH_3COONa, purity of ≥99%, Fisher BioReagents) were used as the electrolyte for the supercapacitor. Acetylene black (CB, purity of >99.9%, Alfa Aesar), polyvinylidene difluoride (PVDF, HSV900, MTI Corporation), polytetrafluoroethylene (PTFE in 60 wt % of aqueous dispersion, MTI Corporation), and 1-methyl-2-pyrrolidinone (NMP, biotech-grade, purity of ≥99.7%, Sigma-Aldrich) were used as the conducting material, binder, and solvent for making the electrode ink. Ethanol (purity of ≥99.9%, Fisher Scientific) was used as the solvent for the ink prepared with PTFE. Whatman glass microfiber filters (934-AH) were used as a separator. Nickel foil (0.01 mm thick, MSE Supplies) was used as a current collector, and stainless-steel coin cell 2032 components, cases (CR2032CASE316), spacers (CR20SPA05), and springs (CR20WS-SPR), were used for making supercapacitor coin cell devices, which were all purchased from MTI Corporation.

2.2. Activated Carbon Synthesis from Waste-Activated Sludge and Spent Coffee. Dried sludge (DS) and dried spent coffee (SC) were ground in a coffee grinder to obtain a fine powder. The mixture of DS and SS was prepared in a 1:1 ratio as the carbon precursor for preliminary evaluation purposes. The mixture of the carbon precursor was combined with different activation agents including K_2CO_3, $Na_2S_2O_3$, and $Na_3C_6H_5O$ and in some cases in the presence of KCl as the molten salt additive, in a mortar and pestle. This method is called the dry method of mixing. After mixing, the mixture was put into a quartz crucible, inserted into a tube furnace (Lindberg Blue, Thermo Scientific), and heated up to 800−900 °C with a ramp rate of 5 °C min^{-1} and a dwell time of 1 h under a nitrogen atmosphere. The schematic of the synthesis process is shown in Supporting Information Figure S1a. To compare the effect of the mixing method, the carbon precursors, activation agents, and the KCl additive were mixed in 20 mL of deionized water (DI) in a beaker at 25 °C overnight (∼18 h). This method is called the wet method. The

https://doi.org/10.1021/acsomega.3c09438
ACS Omega 2024, 9, 13134−13147

Table 1. Summary of the Surface Area and Micropore Analysis of ACs in the Absence/Presence of KCl Synthesized with Sodium Thiosulfate as the Activation Agent at 800 °C

sample	BET surface area ($m^2\ g^{-1}$)	micropore area ($m^2\ g^{-1}$)	mesopore area ($m^2\ g^{-1}$)	total pore volume ($cm^3\ g^{-1}$)	average pore size (nm)
SSC-Blank-800	21 ± 1	5.4 ± 0.3	15.5 ± 0.77	0.05 ± 0.00	9.73 ± 0.09
SSC-$Na_2S_2O_3$-1.5-800	268 ± 13	115 ± 6	148 ± 7	0.38 ± 0.02	5.70 ± 0.05
SSC-$Na_2S_2O_3$-KCl-1.5-3.3-800	683 ± 32	288 ± 14	394 ± 20	0.58 ± 0.03	3.47 ± 0.03
SSC-$Na_2S_2O_3$-KCl-1.5-3.6L-800	878 ± 44	326 ± 16	552 ± 28	0.83 ± 0.04	3.89 ± 0.04

mixture was dried in the oven (Across International) at 80 °C for 24 h to obtain the dried powder before activation in the oven as described above, see Supporting Information Figure S1b. In all cases, the porous carbon materials after activation and cooling to room temperature were washed with DI water, and the solid was collected by using vacuum filtration with a polyamide membrane filter (0.2 μm pore size, Sartorius) and dried in a vacuum oven (Across International) at 80 °C and 25 inHg gauge pressure for 24 h. A blank porous carbon sample was synthesized by self-activation under the same conditions without an activation agent. The effects of the operating temperature, activation agent, mixing procedure, and adding KCl were evaluated on the physiochemical characteristics of the activated carbons (ACs) and their electrochemical performance.

The samples are labeled as SSC-activation agent-KCl-x-y(L)-T throughout the text with legend constituents adjusted depending on the components and conditions as described next: the activation agent with choices of blank (no activation agent), K_2CO_3, $Na_2S_2O_3$, or $Na_3C_6H_5O$; x is the weight mixing ratio of the activation agent with the dried carbon precursor, and T is the activation operating temperature (°C). For example, a sample labeled as SSC-$Na_2S_2O_3$-1.5-800 (Table 1) was processed with $Na_2S_2O_3$ as the activation agent at a 1.5 weight ratio with a carbon precursor and 800 °C. Some samples were processed mixing the activation agent with the KCl additive, labeled as "activation agent-KCl", and in such a case, y is the weight mixing ratio of KCl with the carbon precursor, which could be accompanied with "L" indicating liquid-phase mixing in DI water (wet mixing method). For example, samples labeled as SSC-$Na_2S_2O_3$-KCl-1.5-3.3-800 and SSC-$Na_2S_2O_3$-KCl-1.5-3.6L-800 in Table 1 were processed both with $Na_2S_2O_3$ as the activation agent and the KCl additive, at a 1.5 weight ratio of $Na_2S_2O_3$ with the carbon precursor and 800 °C. One sample contains a 3.3 weight ratio (y) of KCl to carbon and the other 3.6, and the latter one was wet mixed as denoted by the "L" in "3.6L".

2.3. Analytical Techniques. Morphologies of the porous carbon were acquired by scanning electron microscopy (SEM, Zeiss Crossbeam 540). The nitrogen sorption isotherms of the porous carbons were measured at −196 °C by using a Quantachrome Autosorb iQ-MP micropore analyzer. About 60 mg of the AC sample was degassed at 200 °C for 6 h before physisorption to remove the moisture or volatiles trapped in the pores. The specific surface area was calculated by applying the Brunauer−Emmett−Teller (BET) method. The t-plot method was applied to determine the microporous areas. The difference between the BET surface area and the microporous surface was calculated to assess the external surface area, which is the surface covered by the mesopores and micropores. The total pore volume was evaluated at a relative pressure (p/p_o) of 0.99. The pore size distribution (PSD) was determined by using nonlocal density functional theory (NLDFT). Raman spectroscopy (Senterra, Bruker Raman microscope) with an excitation beam wavelength of 532 nm, an integration time of 10 s, a spectra resolution of 3−5 cm^{-1}, and a power level of 2 mW was performed to characterize the chemical nature of the porous carbon samples.

2.4. Electrode Fabrication. AC samples, acetylene black, and PVDF binder were dried in an oven (Across International) at 80 °C for 24 h before slurry preparation. Carbon samples were ground to obtain a fine powder with zirconia balls (1/4 in., Uxcell) at 1500 rpm for 5 min in a SpeedMixer (FlackTek, Inc., DAC150.1 FVZ). The slurry was cast onto Ni foil using the doctor blade (KTQ-II, LianDu-US) technique and dried at 60 °C under vacuum 25 inHg gauge pressure overnight (∼24 h). The AC sample, acetylene black, and PTFE were mixed in ethanol (99.9%, Fisher Scientific) with a mixing ratio of 80:10:10 and coated on the surface of the punched nickel foil (12.7 mm diameter) using the drop casting technique. The coating prepared by the PVDF binder was punched into a diameter of 12.7 mm (area loading ≈ 2−4 mg cm^{-2}, with a 20 μm thickness). The loading was calculated by subtracting the initial mass of the Ni foil from the mass of the coated nickel foil after drying.

2.5. Coin Cell Assembly. Symmetric supercapacitor coin cells were prepared with synthesized AC materials by using MTI coin cell cases made of stainless steel. A pair of 12.7 mm diameters were punched out of the coating. Slightly larger 19 mm Whatman (G/F) glass fiber filters were punched out to be used as a separator. The separator was soaked in 6 M KOH and 1 M CH_3COONa before cell assembly. The coin cells were pressed by using a hydraulic crimper (MSk-110, MTI Corporation) at 100 psi.

2.6. Electrochemical Setup. The electrochemical performance of the AC-based supercapacitor cells (two electrodes) was carried out with a Biologic SP-150 electrochemical workstation at room temperature. Electrodes underwent cyclic voltammetry with a potential window of 0−1 V for 6 M KOH and 0−1.5 V for 1 M CH_3COONa with the scan rate of 20 to 500 mV s^{-1} in KOH and 20−1000 mV s^{-1} in CH_3COONa. In all the cases, the sustained periodic state was achieved after 4 sweeps. The galvanostatic charge−discharge (GCD) measurement was implemented in the range of current to mass ratio of 0.2 to 20 A g^{-1} with the same voltage window for cyclic voltammetry. The electrochemical impedance spectroscopy (EIS) measurements were performed over a frequency range from 200 kHz to 0.1 Hz with a sinusoidal voltage amplitude of 10 mV at the open-circuit potential.

The specific gravimetric capacitance of a single electrode (F g^{-1}) and the cell (C_g, F g^{-1}) was determined from the galvanostatic cycles using eqs 1 and 2 where dV/dt is the slope of the discharge (V s^{-1}) curve after the internal resistance (IR) drop.[29−31]

https://doi.org/10.1021/acsomega.3c09438
ACS Omega 2024, 9, 13134−13147

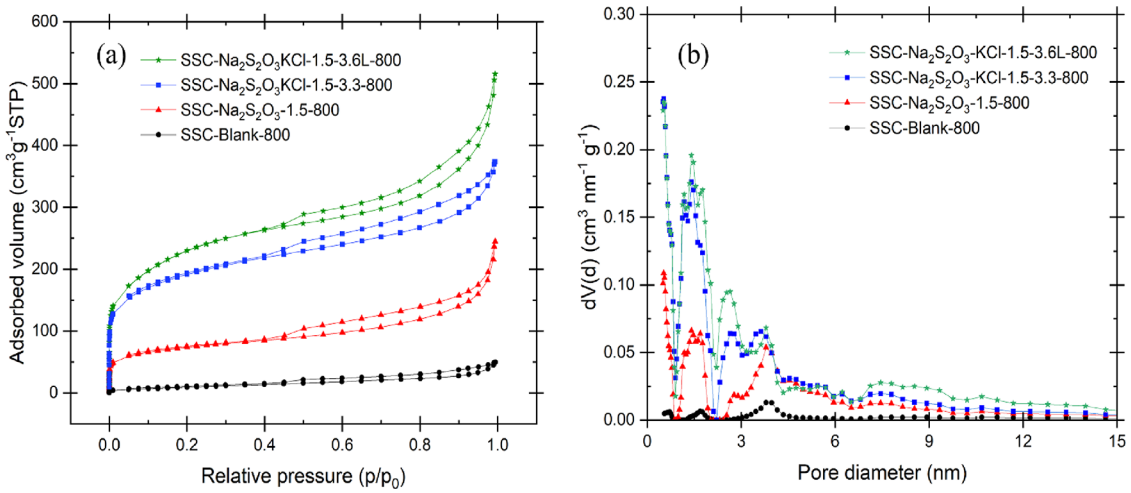

Figure 1. (a) Nitrogen adsorption−desorption isotherms and (b) pore size distribution of the porous carbons synthesized with self-activation and $Na_2S_2O_3$ in the presence of KCl at 800 °C for 1 h under a nitrogen atmosphere. Adding KCl enhanced the surface area by improving the contact between the carbon precursor and the activation agent. Mixing in the liquid phase resulted in a notable enhancement in both the pore volume and surface area.

$$C = \frac{4I}{\left(\frac{dV}{dt}\right)m} \quad (1)$$

$$C_g = \frac{2I\Delta t}{m\Delta V} \quad (2)$$

In these equations, I is the constant current in discharging (A), and m is the milligram mass of the active material on each electrode (g). The Ragone plots were traced by using a galvanostatic discharge test. The specific energy (E, Wh kg^{-1}) and power (P, W kg^{-1}) were calculated by using eqs 3 and 4:

$$E = \frac{C_g \times V_{max}^2}{2 \times 3.6} \quad (3)$$

$$P = \frac{E \times 3600}{\Delta t} \quad (4)$$

where V_{max} is the voltage at the beginning of the discharge and Δt is the discharge time. A factor of 3.6 was used to convert the energy density unit from J g^{-1} to Wh kg^{1-}. For every experimental condition, a pair of coin cells underwent testing, and the associated uncertainties were quantified through the calculation of the standard deviation.

3. RESULTS AND DISCUSSION

3.1. Mechanism of Activation by Adding Potassium Chloride on Physicochemical Properties of the Porous Carbons. In this section, sodium thiosulfate was used as a green activation agent. Sevilla et al. reported that using sodium thiosulfate as the activation agent with a ratio of 1.5 was mixed with the carbon precursor and resulted in the highest surface area for the biomass-based activated carbon.[32] Therefore, the activation agent to carbon precursor ratio of 1.5 was selected for the activation process. It is important to note that potassium chloride (KCl) and sodium thiosulfate ($Na_2S_2O_3$) decomposition products are melted at 800 °C (KCl melting point, 770 °C), and the carbon precursor materials are immersed into the liquid mixture of activation agents. In this condition, melted KCl will play a role as the confinement medium, which leads to reinforcing the contact between the carbon precursor and activation agent decomposition products and enhances the reaction rate.[27] The porous structure of the activated carbon samples was examined by nitrogen physisorption. The adsorption isotherm and pore size distribution are listed in Figure 1. The BET isotherm showed the typical I/IV isotherm indicating the presence of substantial micropores and mesopores in the porous carbon after chemical activation with sodium thiosulfate. The porosity characteristics of the samples such as the BET surface area and pore size distribution are summarized in Table 1. Chemical activation resulted in producing highly porous activated carbons with a significantly higher surface area compared to physical/self-activation (SSC-Blank-800 °C). The specific surface area of AC samples enhanced significantly from 21 ± 1 m^2 g^{-1} for a blank sample to 268 ± 13 m^2 g^{-1} with chemical activation. The BET analysis results indicated that the addition of KCl further increased the surface area and pore volume substantially from 268 ± 13 to 683 ± 32 m^2 g^{-1}. It is theorized that adding KCl leads to the formation of more micro- and mesopores in the activated carbon structure by improving the contact of the activation agent and the carbon precursor. The physisorption analysis demonstrated a higher surface area with a significantly higher pore volume (878 ± 44 m^2 g^{-1} and 0.83 ± 0.04 cm^3 g^{-1}, respectively) and a wider pore diameter by mixing the activation agent and the carbon precursor in the liquid phase overnight (~18 h). Further, SEM imaging of porous carbons was conducted to evaluate the effect of activation on the carbon structure morphology (Supporting Information Figure S2). A blank sample (SSC-Blank-800 °C) synthesized by self-activation shows a smooth surface with no pore development. On the other hand, chemical activation with sodium thiosulfate results in a highly porous structure. The sponge-like carbon structure with interconnect microporous structure was obtained by adding KCl to the mixture. It is worth noting that the formation of mesopores in the carbon structure could improve electrolyte mass transfer through the pores, leading to a higher rate capability.

The activated carbons were further characterized by Raman spectroscopy. The D-band around 1350 cm^{-1} results from sp^3-hybridized defect sites in the carbon structure, representing the structural defects and the disordered structure on the graphitic

https://doi.org/10.1021/acsomega.3c09438
ACS Omega 2024, 9, 13134−13147

carbon.[33,34] The G-band around 1590 cm^{-1} shows the presence of graphitic or ordered planes in the carbon material.[35] The Raman spectra can also verify the defects and disorder degree of the above samples by comparing the D-band and G-band intensity ratio. The ratio of the D- to G-bands (I_D/I_G) is known as the degree of graphitization or defect density, which informs about the crystallinity level of the carbon materials. The Raman spectra of the SSC-Blank-800, SSC-$Na_2S_2O_3$-1.5-800, SSC-$Na_2S_2O_3$-KCl-1.5-3.3-800, and SSC-$Na_2S_2O_3$-KCl-1.5-3.6L-800 represent two distinct peaks around 1343 (D-band) and 1590 cm^{-1} (G-band) (Figure 2).

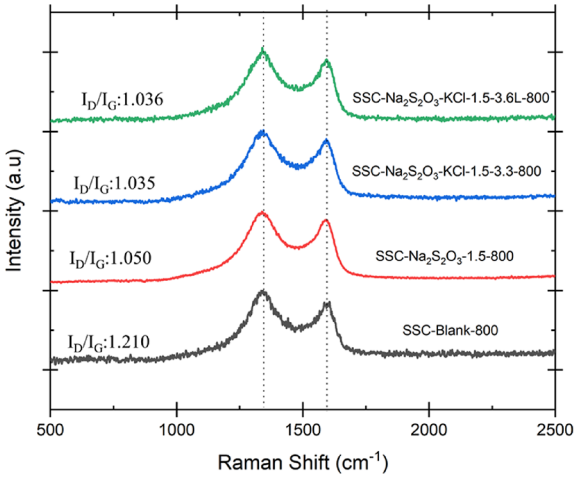

Figure 2. Raman spectra of the activated carbons synthesized by sodium thiosulfate in the presence of KCl at 800 °C. A higher graphitization degree was obtained for all the AC samples activated by sodium thiosulfate compared to self-activation. The increase in the I_D/I_G ratio due to liquid-phase mixing indicates the development of defects/disorders within the carbon structure.

The ratio of the D-band/G-band (I_D/I_G) was calculated to be 1.21 for the SSC-Blank-800 synthesized by self-activation. The I_D/I_Gdecreased to 1.035 by incorporating KCl in the synthesis mixture, which indicates a higher degree of graphitization in the carbon structure. On the other hand, the I_D/I_G slightly increased for the SSC-$Na_2S_2O_3$-KCl-1.5-3.6L-800, which originated from creating more defects into the carbon structure.

3.2. Effect of the Operating Temperature on Physicochemical Properties of the Porous Carbons.

Referring to Table 1, the highest surface area was achieved for the SSC-$Na_2S_2O_3$-KCl-1.5-3.6L at 800 °C. Therefore, the operating temperature was further increased to 850 and 900 °C to study the effect of calcination temperature on the pore size formation and defects in the carbon structure.

Figure 3 represents the BET isotherms of the AC samples synthesized by sodium thiosulfate at different operating temperatures. It is evident that increasing the temperature from 800 to 850 °C resulted in a slight increase in the surface area and an increase in the mesoporous surface area from 482 ± 24 to 552 ± 28 $m^2\ g^{-1}$, see Table 2. As the temperature increased from 850 to 900 °C, the mesoporous surface area decreased to 492 ± 25 $m^2\ g^{-1}$ with a smaller pore size (3.67 nm) due to collapsing of the pores and agglomeration.[36] Table 2 provides a summary of the surface area and microporous specification for ACs synthesized with sodium thiosulfate and KCl at different operating temperatures (800−900 °C). Additional analysis with Raman spectroscopy revealed that elevating the carbonization temperature results in a greater degree of graphitization. The I_D/I_G values of the samples synthesized at 800 °C (1.036) are higher than those of 850 °C (1.031) and the samples synthesized at 900 °C (1.025) showing a greater degree of disorder and defects induced by chemical activation at lower operation temperatures (Figure 4).[35]

3.3. Effect of the Activation Agent on the Physiochemical Properties.

In this study, green chemicals were chosen as the activation agents to prevent post-treatment with an acid, which is typically required to remove impurities. Potassium carbonate, sodium thiosulfate, and trisodium citrate were selected to investigate the impact of various activation agents on the pore formation and specific surface area. Referring to the literature, the primary reactions occurring during activation using potassium carbonate are presented as eqs 5−8:[37]

$$2K_2CO_3 + 4C \rightarrow 6CO + 4K \quad (5)$$

$$K_2CO_3 \rightarrow CO_2 + K_2O \quad (6)$$

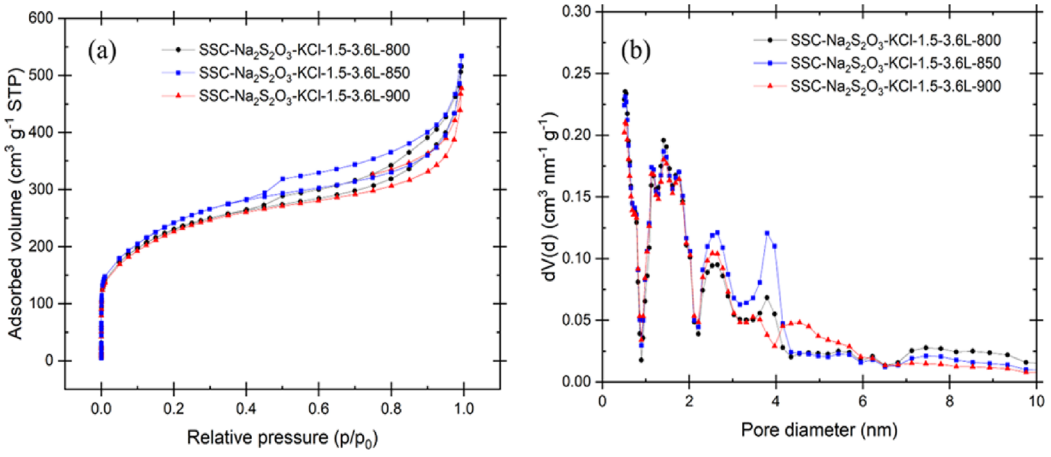

Figure 3. Effect of operation temperature on (a) BET surface area and (b) pore size distribution; the surface area and pore volume increased as the temperature was raised to 850 °C. However, with a further increase in operation temperature to 900 °C, both the surface area and pore volume decrease. The reduction in the pore size at higher operating temperatures is attributed to the collapse of the pores.

https://doi.org/10.1021/acsomega.3c09438
ACS Omega 2024, 9, 13134−13147

Table 2. Summary of the Surface Area and Microporous Specification for the ACs Synthesized with Sodium Thiosulfate and KCl at Different Operating Temperatures (800−900 °C)

sample	BET area ($m^2\ g^{-1}$)	micropore area ($m^2\ g^{-1}$)	mesopore area ($m^2\ g^{-1}$)	total pore volume ($cm^3\ g^{-1}$)	average pore size (nm)
SSC-$Na_2S_2O_3$-KCl-1.5-3.6L-800	820 ± 41	339 ± 17	482 ± 24	0.80 ± 0.04	3.89 ± 0.04
SSC-$Na_2S_2O_3$-KCl-1.5-3.6L-850	878 ± 44	326 ± 16	552 ± 28	0.83 ± 0.04	3.76 ± 0.04
SSC-$Na_2S_2O_3$-KCl-1.5-3.6L-900	806 ± 40	314 ± 17	492 ± 25	0.74 ± 0.04	3.67 ± 0.04

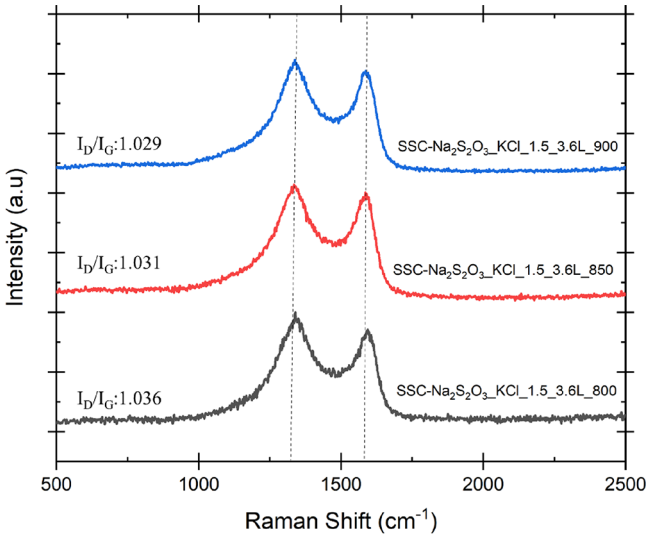

Figure 4. Raman spectra of the activated carbons synthesized at (a) 800 (b) 900, and (c) 850 °C. The ratio of the I_D/I_G band decreased while the temperature increased from 800 to 900 °C resulting in an increase in the graphitizing degree of the porous carbon.

$$CO_2 + C \rightarrow 2CO \quad (7)$$

$$K_2O + C \rightarrow CO + 2K \quad (8)$$

When the temperature rises above 627 °C, K_2CO_3 reacts with carbon (C) to generate carbon monoxide (CO) (eq 5). This reaction contributes to the formation of micropores.[38] K_2CO_3 will undergo thermal decomposition to produce carbon dioxide gas (CO_2) (eq 6) and reacts with C to generate CO gas (eq 7). K_2O from K_2CO_3 decomposition further reacts with C to form CO gas and potassium K (eq 8). The generated K can also be integrated into the carbon structure, causing an expansion of the carbon framework. The subsequent release of CO and CO_2 gases typically leads to the creation of the mesopores.[37] As a result, the carbon obtained through the use of K_2CO_3 activation agents exhibits a structure rich in micropores.

The proposed activation process involving sodium thiosulfate relies on the reaction between the carbon precursor and the sodium sulfate produced from the decomposition of sodium thiosulfate at $T > 250$ °C (eq 9).[27] The oxidation reaction between carbon and sodium sulfate occurs at a temperature above 342 °C, resulting in the production of carbon dioxide (eq 10). Moreover, at an operating temperature above 520 °C, sodium sulfate reacts with carbon to generate carbon monoxide (eq 11).

$$4Na_2S_2O_3 \rightarrow 3Na_2SO_4 + Na_2S_5 \quad (9)$$

$$Na_2SO_4 + 2C \rightarrow Na_2S + 2CO_2 \quad (10)$$

$$Na_2SO_4 + 4C \rightarrow Na_2S + 4CO \quad (11)$$

It is important to note that sodium thiosulfate decomposition products are melted at 800 °C (melting point of Na_2SO_4−Na_2S, 740 °C), and the carbon precursor materials are immersed into the liquid mixture of activation agents. The formation of the liquid phase has a considerable influence on the activation reactions. Likewise, it has been reported that sodium citrate undergoes a transformation to sodium carbonate at temperature of 650 °C, after which sodium carbonate serves as the activation agent.[39] The proposed activation mechanism is presented as follows (eqs 12−15):[40,41]

$$Na_2CO_3 + 2C \rightarrow 2Na + 3CO \quad (12)$$

$$Na_2CO_3 \rightarrow Na_2O + CO_2 \quad (13)$$

$$CO_2 + C \rightarrow CO \quad (14)$$

$$Na_2O + C \rightarrow 2Na + CO \quad (15)$$

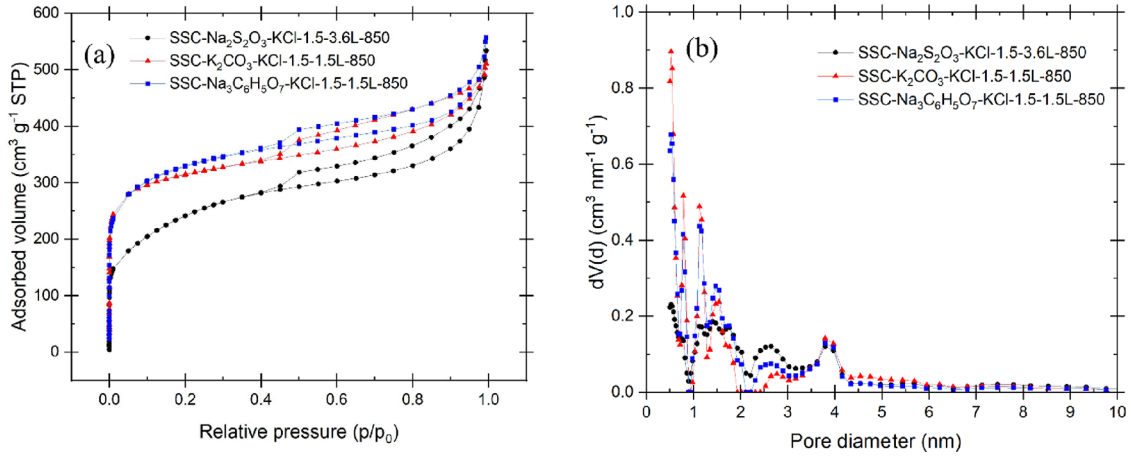

Figure 5. Effect of the activation agent on (a) BET isotherm and (b) pore size distribution. A significantly higher BET and microporous surface area were obtained with potassium carbonate and sodium citrate as the activation agents.

https://doi.org/10.1021/acsomega.3c09438
ACS Omega 2024, 9, 13134−13147

Table 3. Summary of the Surface Area and Pore Volumes for the Synthesized ACs by Different Activation Agents in the Presence of KCl at 850°C

sample	BET area (m^2 g^{-1})	micropore area (m^2 g^{-1})	mesopore area (m^2 g^{-1})	total pore volume (cm^3 g^{-1})	average pore size (nm)
SSC-$Na_2S_2O_3$-KCl-1.5-3.6L-850	878 ± 44	326 ± 16	552 ± 28	0.83 ± 0.04	3.89 ± 0.04
SSC-K_2CO_3-KCl-1.5-1.5L-850	1179 ± 59	860 ± 43	319 ± 16	0.79 ± 0.04	2.68 ± 0.03
SSC-$Na_3C_6H_5O_7$-KCl-1.5-1.5L-850	1198 ± 60	744 ± 37	454 ± 23	0.86 ± 0.04	3.29 ± 0.03

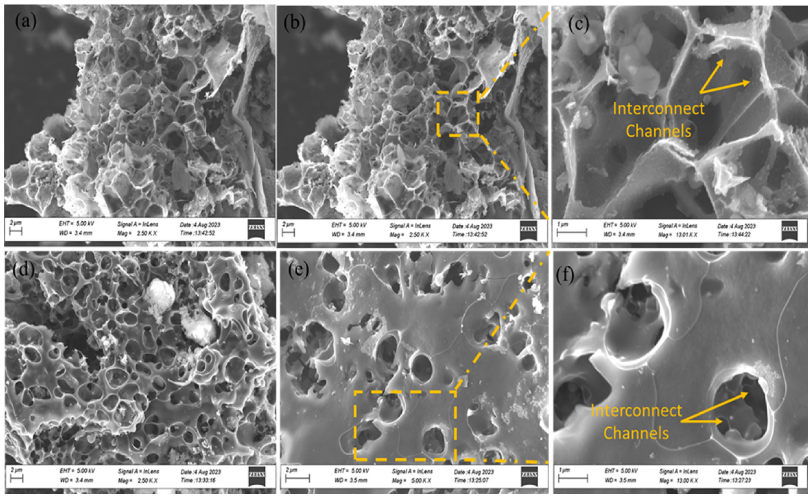

Figure 6. (a–c) Morphology of the AC prepared by potassium carbonate and KCl at 850 °C, 3D honeycomb porous carbon with interconnected micropores; (d–f) morphology of the AC sample prepared by trisodium citrate and KCl at 850 °C, where a hierarchical porous structure with spherical pores was formed.

As mentioned earlier, the greatest surface area was achieved when the temperature was raised to 850 °C, with a KCl to raw material ratio of 3.6. Since potassium chloride does not actively participate in the activation process, the quantity of KCl in the chemical activation for both potassium carbonate and trisodium citrate was reduced to a ratio of 1.5. The proportion of the activating agent to the carbon precursor remained consistent at a ratio of 1.5. Figure 5 shows the BET isotherm and pore size distribution of the activated carbons synthesized by the different activating agents. The highest surface areas of 1179 ± 59 and 1198 ± 60 m^2 g^{-1} were obtained for the samples activated by potassium carbonate and trisodium citrate, respectively. These samples also showed the presence of a substantial amount of the microporous area, which is desirable for supercapacitor application. The percentage of the microporous area to the total BET surface area drastically increased from 37 ± 2 to 73 ± 4 and 62 ± 3% when sodium thiosulfate was replaced with potassium carbonate and trisodium citrate, respectively. This can be explained by the reactions between the activation agent and the carbon precursor, resulting in the development of porous materials. Detailed information about the microporous area is summarized in Table 3.

The surface morphology of the carbons with a higher surface area was analyzed using SEM. Figure 6a–f shows the morphologies of the ACs synthesized from potassium carbonate and trisodium citrate. The hierarchical porous carbon featuring various pore shapes was synthesized using different activation agents. Activation with potassium carbonate resulted in the formation of the three-dimensional (3D) sponge-like morphology with a honeycomb structure, while activation with trisodium citrate led to creation of the spherical holes. It is noted that a substantial number of mesopores and micropores were generated during activation with both chemicals. In addition, it is evident that the larger pores are interconnected with another one through the presence of micropores. This could potentially reduce the electrolyte ion transportation distance leading to higher power and energy density. The effect of activation agents on the defect/graphitization degree of the AC samples was studied via Raman spectra and is presented in Supporting Information Figure S3. The I_D/I_G ratios of 1.036, 0.98, and 1.05 were obtained for AC samples synthesized using sodium thiosulfate, potassium carbonate, and trisodium citrate, respectively. The higher value of I_D/I_G was obtained for trisodium citrate due to the development of more structural defects compared with other activation agents. However, the AC sample synthesized with potassium carbonate exhibits a slightly greater degree of graphitization.

3.4. Electrochemical Performance of the Biomass-Derived Porous Carbons. *3.4.1. Effect of Adding KCl and a Binder Material.* The binder plays a crucial role in providing effective physical contact between the active carbon particles and establishing a strong adhesion to the current collector. PTFE and PVDF are the commercial binders used for the electrode fabrication. PTFE is an environmentally friendly water-based binder, while PVDF is a nonaqueous binder that requires the use of an NMP solvent to make a slurry for coating.

The effect of the binder on the electrochemical performance of the supercapacitors was evaluated. Cyclic voltammetry experiments were conducted on the synthesized carbons within the range of 20–500 mV s^{-1} to evaluate the effect of the binder on the rate capability. Figure 7 shows the CVs for the AC samples synthesized using sodium thiosulfate and KCl at 800 °C (SSC-$Na_2S_2O_3$-KCl-1.5-3.3-800) with a mixing ratio of

https://doi.org/10.1021/acsomega.3c09438
ACS Omega 2024, 9, 13134–13147

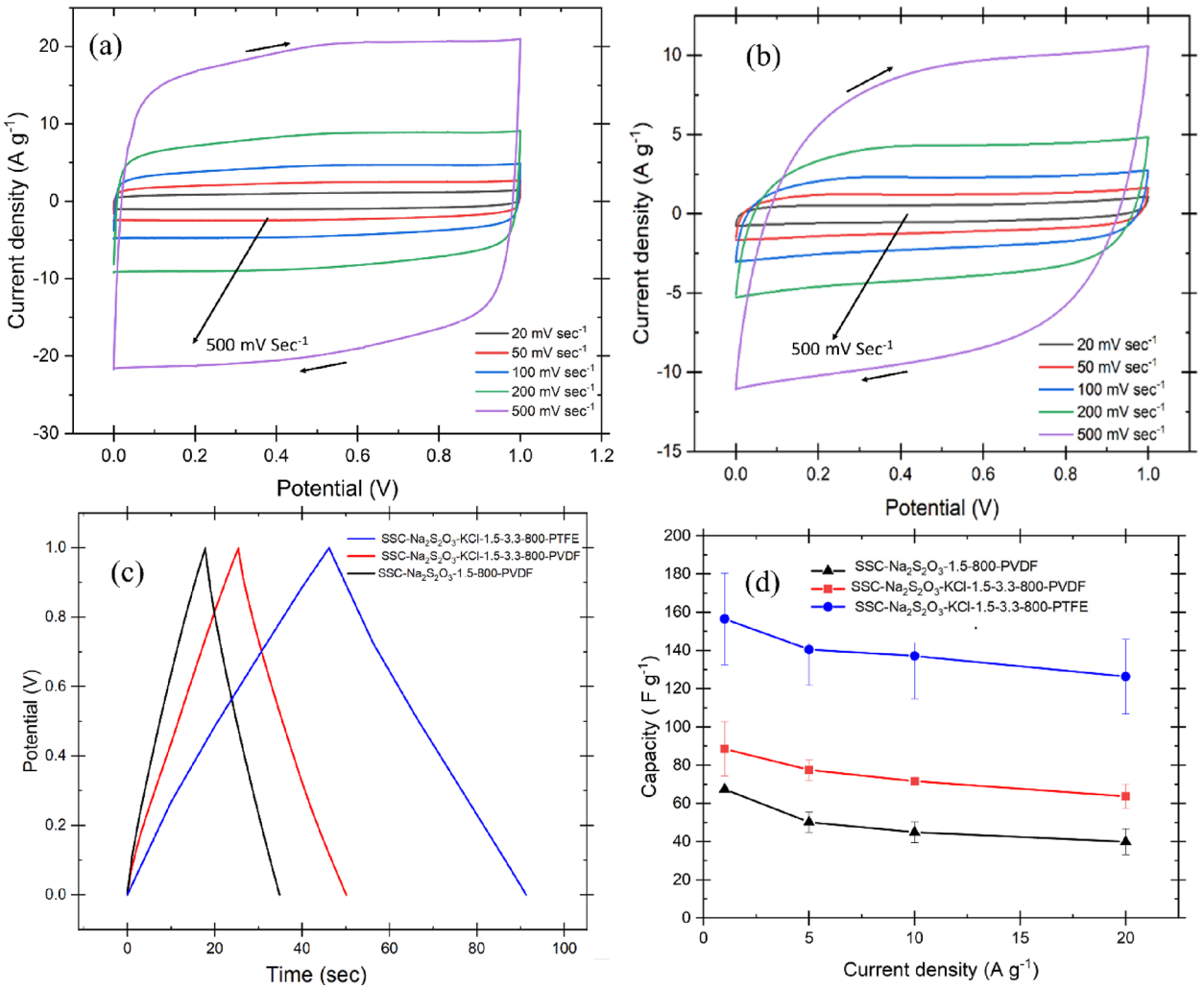

Figure 7. Electrochemical performance of activated carbon in a two-electrode system in 6 M KOH synthesized using sodium thiosulfate and KCl at 800 °C for 1 h (SSC-$Na_2S_2O_3$-KCl-1.5-3.3-800): (a) cyclic voltammogram for the electrode (80:10:10 PTFE) at a scan rate of 20−500 mV s^{-1}, (b) cyclic voltammogram for the electrode (80:10:10 PVDF) at a scan rate of 20−500 mV s^{-1}, (c) effect of KCl and binder on galvanostatic charge/discharge at 1 A g^{-1} in a two-electrode system in 6 M KOH, and (d) electrode capacity at different current densities ranging from 1 to 20 A g^{-1}. A higher capacity was obtained by adding KCl to the activation mixture. The utilization of a PTFE binder demonstrated a significant improvement in the capacity.

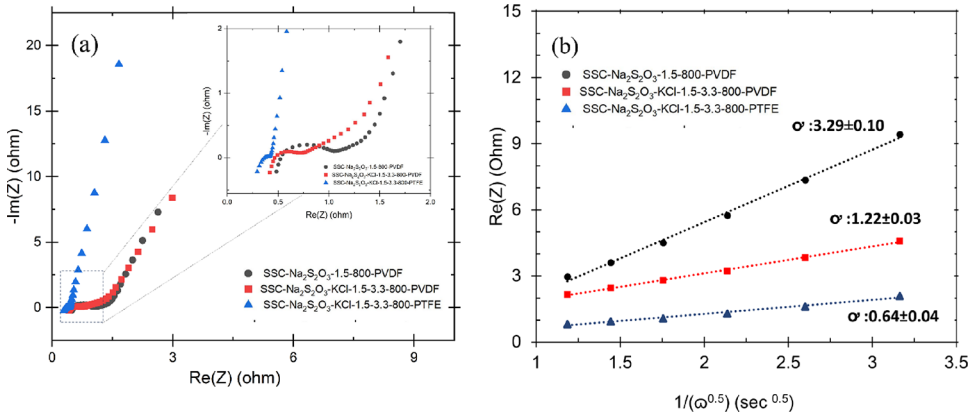

Figure 8. (a) Effect of KCl and binder material on Nyquist plots of the AC electrodes synthesized by sodium thiosulfate at 800 °C in a frequency ranging from 200 kHz to 0.1 Hz. (b) Re(Z) as the function of $1/\sqrt{\omega}$. Adding KCl improves both charge transfer and mass transfer processes by developing more pores in the AC structure. The PTFE binder led to a significant reduction in ESR, R_{CT}, and Warburg coefficient, primarily by improving the wettability of the electrode surface.

https://doi.org/10.1021/acsomega.3c09438
ACS Omega 2024, 9, 13134−13147

80:10:10 (activated carbon:conductive carbon:binder) using different binder materials (PVDF and PTFE). The sample using PTFE shows a larger area as observed under the curve for CV at the same scan rate compared with PVDF, which leads to a higher electrode capacity. The shape of the CV curves remained consistent while the scan rate increased from 20 to 500 mV s^{-1}, indicating the high rate capability of the materials for the fast charge/discharge rate. When the scan rate increased, a significant difference was observed between PVDF and PTFE. This suggests that the ion diffusion is slower in PVDF compared to the PTFE electrode.[42]

Supporting Information Figure S4 shows a cyclic voltammogram comparison of AC samples synthesized using sodium thiosulfate and potassium chloride at 800 °C. The area under CV significantly increased by incorporating KCl, which results in enhancing the electrode capacity. This could be attributed to modification of the textural properties of the AC samples. The galvanostatic charge/discharge cycle was performed to evaluate the effect of adding KCl and different binders on the capacity of the electrode materials (Figure 7c,d). The addition of KCl led to an increase in electrode capacity from 67.4 ± 0.4 to 89 ± 14 F g^{-1} at the current density of 1 A g^{-1}. When PTFE was employed as the binder, the capacity significantly improved to 157 ± 24 F g^{-1} at 1 A g^{-1}, which is higher than that of the commercial activated carbon YP-50F (125 F g^{-1} at 1 A g^{-1}).[43] This is due to an enhancement in the hydrophilicity of the electrode's surface.[33]

Electrochemical impedance spectroscopy (EIS) is a powerful method for studying the electrochemical characteristics of the electrode and its interface. The Nyquist plot shows two primary regions for the supercapacitors: (1) at the high frequency, a semicircle indicating the charge transfer resistance (R_{CT}), and (2) at the low frequency, a vertical line representing the mass transfer resistance. The equivalent series resistance (ESR) is calculated from the intersection of the semicircle with the x-axis at the high frequency. ESR stands for the resistance observed within the electrode, electrolyte, and electrical contact. Figure 8a shows the Nyquist plots for the coin cells made with AC materials synthesized by sodium thiosulfate and KCl with different binders. With the addition of KCl, both ESR and R_{CT} decreased significantly from 0.54 ± 0.04 to 0.47 ± 0.00 and 0.82 ± 0.29 to 0.31 ± 0.05 Ω, respectively. A substantial reduction in ESR and R_{CT} (0.4 ± 0.0 and 0.1 ± 0.1 Ω) was achieved when using the PFTE binder. These results illustrate the key role of the wettability of the electrode surface in the supercapacitor performance. In addition, it is important to emphasize that both ESR and R_{CT} are the key factors for the high specific power in supercapacitors. The findings from EIS analysis are summarized in Table 4. The presence of the vertical line at low frequencies indicates the capacitive characteristics of the cells. Mass transfer information was derived from the Nyquist plot at low frequencies. Warburg resistance illustrates the diffusion of electrolyte ions into porous carbon. The analysis of the impedance as a function of the reciprocal of the square root of frequency was performed to obtain information about the Warburg coefficient σ. Warburg coefficients were determined from the slopes of the linear fitting lines of Re(Z) as the function of $1/\sqrt{\omega}$ representing ion diffusion resistance.[44] Figure 8b shows the fitting data for the Warburg coefficient of the supercapacitor cells. The effect of adding KCl and using different binders on the mass transfer coefficient was studied. Incorporating KCl leads to a notable reduction in the Warburg coefficient from 3.29 ± 0.10 to 1.22 ± 0.03 Ω $s^{-0.5}$. This result aligns with the physical characteristics of the ACs. ACs synthesized using sodium thiosulfate in the presence of KCl showed a substantially higher surface area and pore volume, facilitating the mass transfer and reducing the resistance. The effect of using different binders on the mass transfer resistance was also evaluated. The electrode made with the PTFE binder (10 wt %) exhibited a notably lower Warburg coefficient when compared to the electrode using a PVDF binder (10 wt %). The reduction from 1.22 ± 0.03 to 0.64 ± 0.04 Ω $s^{-0.5}$ is correlated to higher hydrophilicity of the electrode surface, which, in turn, improves the ion transfer into the pores.[33]

Table 4. Summary of the Impedance Resistance for the Supercapacitors Made from ACs Modified by KCl at 800 °C with Different Binders

AC sample	R_{CT} (Ω)	ESR (Ω)	O' (Ω $s^{-0.5}$)
SSC-$Na_2S_2O_3$-1.5-800-PVDF	0.82 ± 0.29	0.54 ± 0.04	3.29 ± 0.10
SSC-$Na_2S_2O_3$-KCl-1.5-3.3-800-PVDF	0.31 ± 0.05	0.47 ± 0.00	1.22 ± 0.03
SSC-$Na_2S_2O_3$-KCl-1.5-3.3-800-PTFE	0.10 ± 0.09	0.37 ± 0.00	0.64 ± 0.04

3.4.2. Effect of the Activation Agent on the Electrochemical Performance of Supercapacitors in a Green Electrolyte. A higher energy density could be achieved by implementing electrolytes with a wider voltage stability window (>1 V). Recent work accomplished by Dyatkin et al. revealed that using sodium acetate at the concentration of 1 M resulted in higher capacity compared to sodium sulfate with the same concentration.[45] Moreover, sodium acetate is a more environmentally friendly electrolyte. Therefore, the effect of the activation agent on the electrochemical performance of the supercapacitors was evaluated in a two-electrode system in 1 M sodium acetate (CH_3COONa). To evaluate the stable operating potential window in CH_3COONa, cyclic voltammetry at 100 mV s^{-1} was performed in the range of 1−1.5 V. Figure 9a shows the cyclic voltammogram for the SSC-$Na_3C_6H_5O_7$-KCl-1.5-1.5L-850 in a 1 M CH_3COONa electrolyte. It is clear that employing sodium acetate enables the expanded operation potential window up to 1.5 V, in contrast to traditional aqueous solutions (6 M KOH), where the operating potential is limited to 1 V. Therefore, significantly higher energy density will be achieved in supercapacitors. It has been reported that the desolvated anion diameter is 0.15 nm for CH_3COO^- (0.71 nm, while it is solvated);[45] therefore, all the ions, even the fully solvated ones, could fit into the majority of the activated carbon pores.

To study the rate capability of the AC electrodes in the CH_3COONa electrolyte, cyclic voltammetry with a scan rate of 20−1000 mV s^{-1} and galvanostatic charge/discharge were performed at the current density of 0.2−20 A g^{-1}. Supporting Information Figure S5 shows the electrochemical performance of the AC electrodes activated by trisodium citrate and potassium carbonate in 1 M CH_3COONa. The shape of the cyclic voltammetry curve was still rectangular even at a higher scan rate (1000 mV s^{-1}) showing the substantial rate capability performance. Likewise, the galvanostatic charge/discharge curve represented a triangular shape even at a high current density of 20 A g^{-1} with a negligible IR drop (Supporting Information Figure S6). The charge transfer mechanism in the supercapacitor can be evaluated from eq 16:[46]

https://doi.org/10.1021/acsomega.3c09438
ACS Omega 2024, 9, 13134−13147

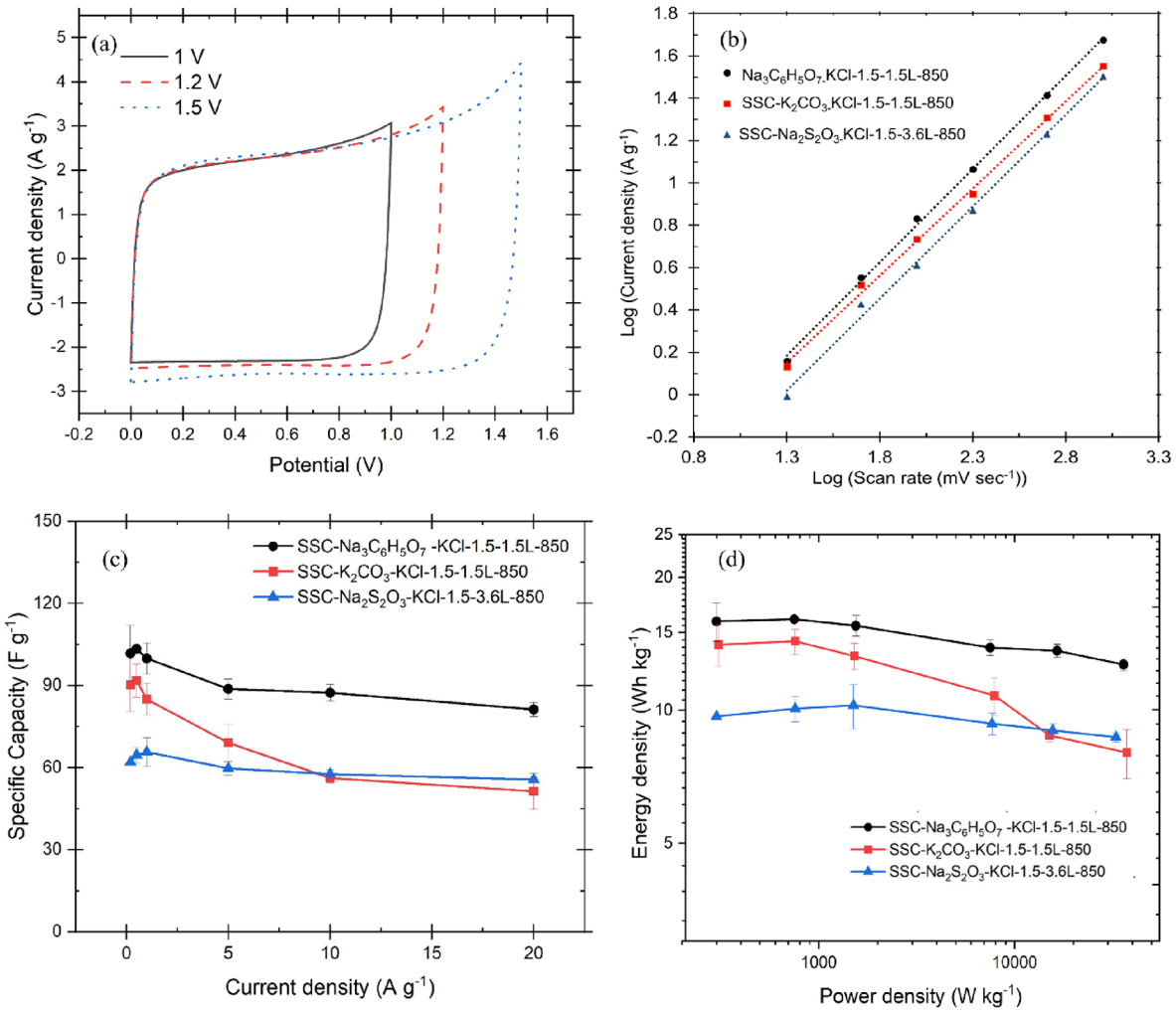

Figure 9. (a) Cyclic voltammetry of the supercapacitor made with AC synthesized by trisodium citrate and KCl at 850 °C for 1 h with 1 M sodium acetate as the electrolyte at 100 mV s^{-1} at the operating potential window of 1−1.5 V, (b) *b* values for fast kinetic evaluation as the function of the scan rate at 20−1000 mV s^{-1}, (c) specific capacity as the function of current density at 0.2−20 A g^{-1}, and (d) Ragone plot of the symmetric supercapacitor in a 1 M sodium acetate electrolyte. A maximum specific capacity of 101.8 ± 10.2 F g^{-1} was obtained for $Na_3C_6H_5O_7$-KCl-1.5-1.5L-850 at 0.2 A g^{-1} corresponding to a 15.9 ± 1.6 Wh kg^{-1} energy density and a 300.00 ± 0.01 W kg^{-1} power density. The maximum power density of 36.05 ± 1.2 kW kg^{-1} was achieved at 10 A g^{-1} for the $Na_3C_6H_5O_7$-KCl-1.5-1.5L-850.

$$i = av^b \quad (16)$$

where *i* is the peak current (A), *v* is the scan rate (mV s^{-1}), and *a* and *b* are coefficients.[46] To understand the rate capability and kinetic information, log(*i*) from cyclic voltammetry data versus the scan rate (mV s^{-1}) was plotted. The slope of the linear fitted line provides kinetic information about the electrochemical reactions by which charge storage can be controlled. There are two well-defined conditions for the slope value. If the slope is equal to 0.5, it means diffusion-controlled phenomena, while the slope equal or close to 1 represents the surface fast charge/discharging of the double-layer supercapacitor.[46] The *b* values of 0.89 ± 0.02, 0.82 ± 0.02, and 0.86 ± 0.02 were obtained for SSC-$Na_3C_6H_5O_7$-KCl-1.5-1.5L-850, SSC-K_2CO_3-KCl-1.5-1.5L-850, and SSC-$Na_2S_2O_7$-KCl-1.5-3.6L-850, respectively, under scan rates from 20 to 1000 mV s^{-1} in 1 M CH_3COONa. The uncertainty of the slopes was calculated with the LINEST function (least-squares method) in Excel. These findings reveal that energy storage in the supercapacitors is achieved through fast charge−discharge at the electro/electrolyte interface for the SSC-$Na_3C_6H_5O_7$-KCl-1.5-1.5L-850 and SSC-K_2CO_3-KCl-1.5-1.5L-850 electrode materials. However, the *b* value decreased to 0.82 ± 0.02 for SSC-$Na_2S_2O_7$-KCl-1.5-3.6L-850, implying that the diffusion-controlled process also contributes to the electrode reaction. The AC synthesized using trisodium citrate showed a higher coefficient that is aligned with the porous structure of carbon (a BET higher surface area with more pore volume). A bigger average pore size of 3.29 ± 0.03 nm was formed using trisodium citrate as the activation agent, which facilitates the ion transfer compared to AC synthesized with potassium carbonate (2.68 ± 0.03 nm).

The electrochemical performance of the symmetric supercapacitors was further evaluated by galvanostatic charge−discharge for the range of current densities of 0.2−20 A g^{-1}. Figure 9c shows the electrode-specific capacitance as a function of current density. The $Na_3C_6H_5O_7$-KCl-1.5-1.5L-850 achieved the highest specific capacity of 101.8 ± 10.2 F g^{-1} when operated at 0.2 A g^{-1}.This translates to an energy density of 15.9 ± 1.6 Wh kg^{-1} for the symmetric cell, which is significantly higher than that of the traditional aqueous electrolyte (2−10 Wh kg^{-1}).[9,47−49] The high capacity resulted from the physicochemical properties of the AC supported by

https://doi.org/10.1021/acsomega.3c09438
ACS Omega 2024, 9, 13134−13147

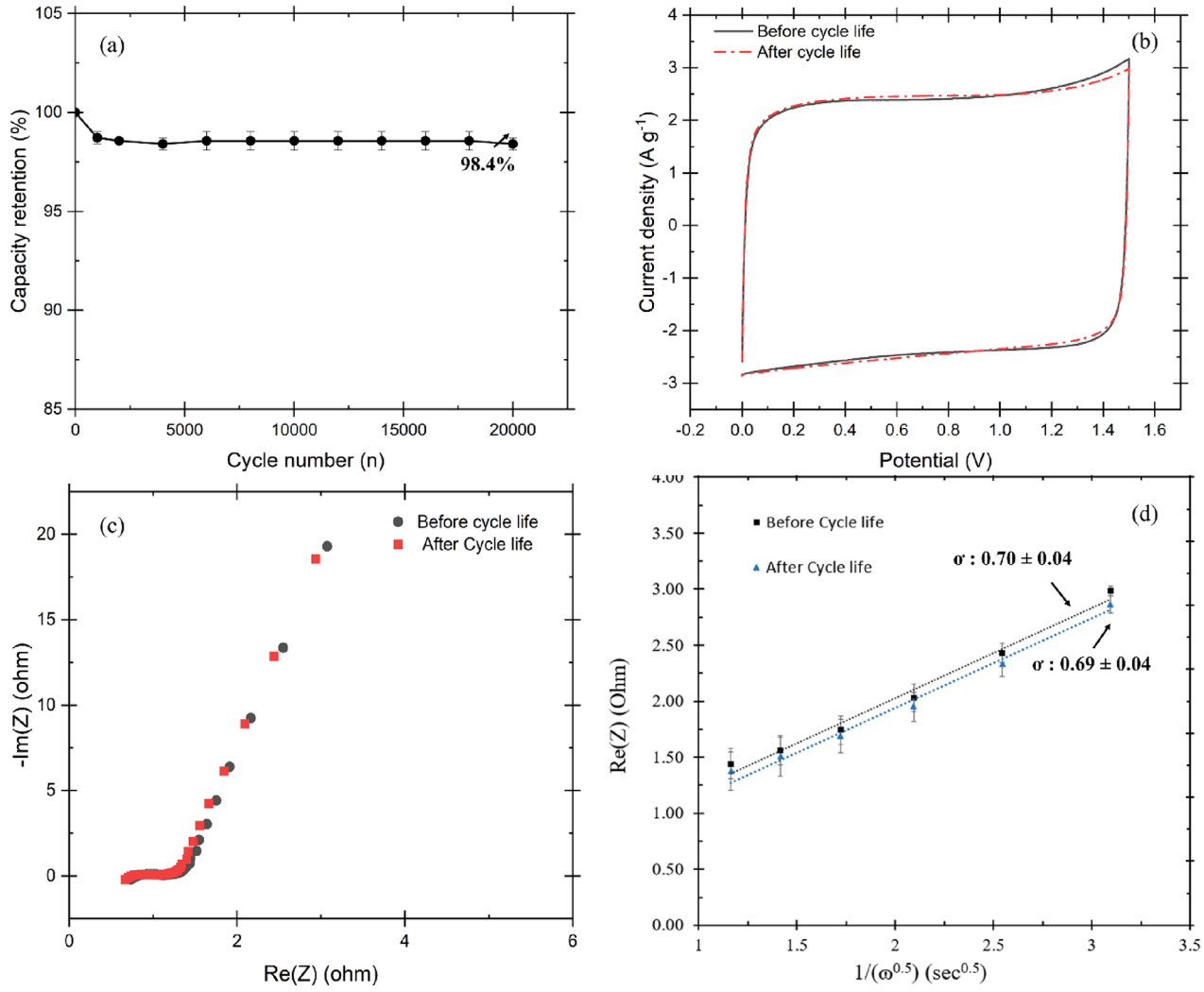

Figure 10. Stability analysis of the SSC-$Na_3C_6H_5O_7$-KCl-1.5-1.5L-850: (a) capacity retention over 20,000 cycles at 10 A g^{-1} in a sodium acetate electrolyte, (b) cyclic voltammetry of the supercapacitor at 100 mV s^{-1} before and after cycle stability at 10 A g^{-1} for 20,000 cycles showing the substantial stability of the supercapacitor, (c) Nyquist plot of the supercapacitor before and after the stability test, and (d) Warburg coefficient analysis. A 98.4 ± 0.3% capacity retention was achieved after a long cycle life test indicating superior stability of the AC electrode. The CV, Nyquist plot, and Warburg coefficient showed a negligible change, revealing that the intrinsic parameter remains stable.

BET surface analysis (1198 ± 60 m^2 g^{-1} and 0.86 ± 0.04 cm^3 g^{-1} pore volume). the high rate charge/discharge process deteriorates the charge storage capability due to the limited time for electrolyte ion diffusion through the electrode pores.[50] In this study, the rate capability of the electrodes was assessed from 0.2 to 20 A g^{-1}. The supercapacitors showed different capacity retentions as a function of current density due to their physical pore structures. Supercapacitors with the AC electrodes synthesized with sodium thiosulfate with a wider pore size (3.89 ± 0.04 nm) showed the highest capacity retention of 89.7 ± 1.6% at 20 A g^{-1}. This was followed by 80.4 ± 5.6 and 56.8 ± 1.2% for trisodium citrate and potassium carbonate with the average pore sizes of 3.29 ± 0.03 and 2.68 ± 0.02 nm. The decrease in the capacitance when the current density is increased to 20 A g^{-1} is related to the resistance of the ion transfer within the pores. The superior capacity retention of the electrodes indicates a fast ion diffusion rate. These findings revealed that both the surface area and pore size distribution are key factors for supercapacitor performance. Figure 9d demonstrates the Ragone plot for supercapacitors with AC electrodes synthesized by different activation agents. The maximum energy density of 15.9 ± 1.6 Wh kg^{-1} was achieved for the $Na_3C_6H_5O_7$-KCl-1.5-1.5L-850 electrode at 0.2 A g^{-1} followed by 14.1 ± 1.5 and 9.70 ± 0.02 Wh kg^{-1} for SSC-K_2CO_3-KCl-1.5-1.5L-850 and SSC-$Na_2S_2O_7$-KCl-1.5-3.6L-850, respectively.

Cycle stability at a high current density is an essential parameter for supercapacitor performance evaluation. The long-term cycle stability was carried out at 10 A g^{-1} for the most promising porous carbon (e.g., SSC-$Na_3C_6H_5O_7$-KCl-1.5-1.5L-850) for 20,000 charge/discharge cycles in 1 M sodium acetate (Figure 10). The supercapacitor showed superior stability, maintaining 98.4 ± 0.3% capacity after a prolonged cycle life. This performance surpasses studies reported in the literature using biomass-derived AC supercapacitors.[51−54] For instance, Liu et al. reported the electrochemical stability of biomass-derived activated carbon in 6 M KOH with a 96% capacity retention at 10 A g^{-1} for 10,000 cycles.[55] Wu et al. reported a cycle stability of 85.2% at 10 A g^{-1} in 6 M KOH for 5,000 cycles.[51] Cyclic voltammetry at 100 mV s^{-1} and electrochemical impedance spectroscopy (200 kHz to 0.1 Hz) were performed before and after cycle life. The

https://doi.org/10.1021/acsomega.3c09438
ACS Omega 2024, 9, 13134−13147

negligible change in EIS and CV shows excellent stability of the electrode materials (Figure 10b,c). The Warburg coefficient (Figure 10d) showed a minor decrease after 20,000 charge/discharge cycles, representing the robust stability of the electrode materials. This finding indicates that the intrinsic properties of the electrode remained unchanged, which is a crucial factor in supercapacitor applications.

4. CONCLUSIONS

In this study, highly porous activated carbon was developed from a sustainable, green route by utilizing eco-friendly activation agents such as sodium thiosulfate, potassium carbonate, trisodium citrate, and inert molten salt (potassium chloride). The effect of activation agents, temperature, mixing procedure, and molten salt additive on the physiochemical properties of the activated carbon samples was studied. The study showed that mixing ingredients in the liquid phase compared to dry mixing before calcination at elevated temperatures leads to a higher surface area and wider pore size. Synthesis temperatures above 900 °C represented an adverse effect on pore formation. The highest mesopore surface area and pore volume were obtained at 850 °C in the presence of trisodium citrate and potassium chloride. The effect of a binder and molten salt on the electrochemical performance of the supercapacitor made from these activated carbon electrodes was investigated. The electrochemical tests indicated that PTFE as a binder not only improved the electrode capacity significantly but also reduced the mass transfer resistance substantially. It is worth noting that sodium acetate as a green, environmentally friendly electrolyte was evaluated for the first time in the long cycle life test. The sodium acetate electrolyte enabled the supercapacitor to operate at a wider operating potential (1.5 V), which results in a higher energy density compared to the traditional aqueous electrolyte (6 M KOH). The electrode maintained an excellent cycle stability of 98.4 ± 0.3% at 10 A g^{-1}. Future investigation into the binder composition, the activation agent ratio to the carbon precursor, and the mixing ratio of the biomass precursors on the electrochemical performance of the supercapacitor is recommended. Optimization of the yield for the activated carbon material is recommended for future work. This work provides a new step toward sustainable electrodes and electrolytes for safe and high-performance supercapacitors in the future.

■ ASSOCIATED CONTENT

Supporting Information

The Supporting Information is available free of charge at https://pubs.acs.org/doi/10.1021/acsomega.3c09438.

Schematic of the porous carbon synthesis process; SEM images of porous carbon samples; Raman spectra for the activated carbons synthesized by trisodium citrate, potassium carbonate, and sodium thiosulfate at 850 °C; cyclic voltammogram comparison at 200 mV s^{-1} in 6 M KOH in a two-electrode system of SSC-$Na_2S_2O_3$-1.5-800 and SSC-$Na_2S_2O_3$-KCl-1.5-3.3-800 with different binders; effect of the activation agent on the electrochemical performance of the supercapacitor in 1 M CH_3COONa; galvanostatic charge/discharge of the supercapacitor made with SSC-$Na_3C_6H_5O_7$-KCl-1.5-1.5-850 and the PVDF binder at 10 and 20 A g^{-1} (PDF)

■ AUTHOR INFORMATION

Corresponding Author

Gerardine G. Botte − *Chemical and Electrochemical Technology and Innovation Laboratory, Institute for Sustainability and Circular Economy, Department of Chemical Engineering, Edward E. Whitacre Jr. College of Engineering, Texas Tech University, Lubbock, Texas 79409, United States;* orcid.org/0000-0002-5678-6669; Email: gerri.botte@ttu.edu

Author

Maasoomeh Jafari − *Chemical and Electrochemical Technology and Innovation Laboratory, Institute for Sustainability and Circular Economy, Department of Chemical Engineering, Edward E. Whitacre Jr. College of Engineering, Texas Tech University, Lubbock, Texas 79409, United States*

Complete contact information is available at: https://pubs.acs.org/10.1021/acsomega.3c09438

Author Contributions

M.J. performed conceptualization, methodologies, investigation, formal analysis, and original draft preparation. G.G.B. performed conceptualization, methodologies, supervision, funding acquisition, and review and editing of the manuscript.

Funding

Financial support was provided by the Chemical and Electrochemical Technology and Innovation Laboratory (CETI), Institute for Sustainability and Circular Economy, at Texas Tech University, the Whitacre Endowed Chair in Sustainable Energy, and the National Science Foundation, EEC Division of Engineering Education and Centers, NSF Engineering Research Center for Advancing Sustainable and Distributed Fertilizer production (CASFER), NSF 20-553 Gen-4 Engineering Research Centers award no. 2133576.

Notes

The authors declare no competing financial interest.

■ ACKNOWLEDGMENTS

The authors would like to acknowledge the personnel from the Lubbock Municipal Wastewater Treatment Plant for access to sludge samples.

■ REFERENCES

(1) Forouzandeh, P.; Kumaravel, V.; Pillai, S. C. Electrode Materials for Supercapacitors: A Review of Recent Advances. *Catalysts* **2020**, *10*, 969.

(2) Olabi, A. G.; Abbas, Q.; Al Makky, A.; Abdelkareem, M. A. Supercapacitors as next generation energy storage devices: Properties and applications. *Energy* **2022**, *248*, No. 123617.

(3) Wang, Z.; Shen, D.; Wu, C.; Gu, S. State-of-the-art on the production and application of carbon nanomaterials from biomass. *Green Chem.* **2018**, *20*, 5031−5057.

(4) Rufford, T. E.; Hulicova-Jurcakova, D.; Zhu, Z.; Lu, G. Q. Empirical Analysis of the Contributions of Mesopores and Micropores to the Double-Layer Capacitance of Carbons. *J. Phys. Chem. C* **2009**, *113*, 19335−19343.

(5) Yin, J.; Zhang, W.; Alhebshi, N. A.; Salah, N.; Alshareef, H. N. Synthesis Strategies of Porous Carbon for Supercapacitor Applications. *Small Methods* **2020**, *4*, 1900853.

(6) Al Rai, A.; Yanilmaz, M. High-performance nanostructured bio-based carbon electrodes for energy storage applications. *Cellulose* **2021**, *28*, 5169−5218.

(7) Bi, Z.; Kong, Q.; Cao, Y.; Sun, G.; Su, F.; Wei, X.; Li, X.; Ahmad, A.; Xie, L.; Chen, C.-M. Biomass-derived porous carbon materials with different dimensions for supercapacitor electrodes: a review. *J. Mater. Chem. A* **2019**, *7*, 16028−16045.
(8) Chen, H.; Wang, G.; Chen, L.; Dai, B.; Yu, F. Three-Dimensional Honeycomb-Like Porous Carbon with Both Interconnected Hierarchical Porosity and Nitrogen Self-Doping from Cotton Seed Husk for Supercapacitor Electrode. *Nanomaterials* **2018**, *8*, 412.
(9) Duan, B.; Gao, X.; Yao, X.; Fang, Y.; Huang, L.; Zhou, J.; Zhang, L. Unique elastic N-doped carbon nanofibrous microspheres with hierarchical porosity derived from renewable chitin for high rate supercapacitors. *Nano Energy* **2016**, *27*, 482−491.
(10) Jung, S.; Myung, Y.; Kim, B. N.; Kim, I. G.; You, I.-K.; Kim, T. Activated Biomass-derived Graphene-based Carbons for Supercapacitors with High Energy and Power Density. *Sci. Rep.* **2018**, *8*, 1915.
(11) Keppetipola, N. M.; Olivier, C.; Toupance, T.; Cojocaru, L. Biomass-derived carbon electrodes for supercapacitors and hybrid solar cells: towards sustainable photo-supercapacitors, Sustain. *Energy Fuels* **2021**, *5*, 4784−4806.
(12) Zhou, S.; Zhou, L.; Zhang, Y.; Sun, J.; Wen, J.; Yuan, Y. Upgrading earth-abundant biomass into three-dimensional carbon materials for energy and environmental applications. *J. Mater. Chem. A* **2019**, *7*, 4217−4229.
(13) Li, F.; Morris, M.; Chan, K.-Y. Electrochemical capacitance and ionic transport in the mesoporous shell of a hierarchical porous core−shell carbon structure. *J. Mater. Chem.* **2011**, *21*, 8880−8886.
(14) Mariana; Marwan; Mulana, F.; Yunardi; Ismail, T. A.; Hafdiansyah, M. F. Activation and characterization of waste coffee grounds as bio-sorbent. *IOP Conf. Ser.: Mater. Sci. Eng.* **2018**, *334*, No. 012029.
(15) Jafari, M.; Botte, G. G. Electrochemical treatment of sewage sludge and pathogen inactivation. *J. Appl. Electrochem.* **2021**, *51*, 119−130.
(16) Kamil, M.; Ramadan, K. M.; Awad, O. I.; Ibrahim, T. K.; Inayat, A.; Ma, X. Environmental impacts of biodiesel production from waste spent coffee grounds and its implementation in a compression ignition engine. *Sci. Total Environ.* **2019**, *675*, 13−30.
(17) Ferrentino, R.; Langone, M.; Fiori, L.; Andreottola, G. Full-Scale Sewage Sludge Reduction Technologies: A Review with a Focus on Energy Consumption. *Water* **2023**, *15*, 615.
(18) Shen, Y.; Linville, J. L.; Urgun-Demirtas, M.; Mintz, M. M.; Snyder, S. W. An overview of biogas production and utilization at full-scale wastewater treatment plants (WWTPs) in the United States: Challenges and opportunities towards energy-neutral WWTPs. *Renew. Sustain. Energy Rev.* **2015**, *50*, 346−362.
(19) US EPA *Inventory of U.S. Greenhouse Gas Emissions and Sinks*, 2017. https://www.epa.gov/ghgemissions/inventory-us-greenhouse-gas-emissions-and-sinks.
(20) Liu, Y.; Liu, P.; Li, L.; Wang, S.; Pan, Z.; Song, C.; Wang, T. Fabrication of biomass-derived activated carbon with interconnected hierarchical architecture via H3PO4-assisted KOH activation for high-performance symmetrical supercapacitors. *J. Electroanal. Chem.* **2021**, *903*, No. 115828.
(21) Yi, J.; Qing, Y.; Wu, C.; Zeng, Y.; Wu, Y.; Lu, X.; Tong, Y. Lignocellulose-derived porous phosphorus-doped carbon as advanced electrode for supercapacitors. *J. Power Sources* **2017**, *351*, 130−137.
(22) Lima, R. M. A. P.; dos Reis, G. S.; Thyrel, M.; Alcaraz-Espinoza, J. J.; Larsson, S. H.; de Oliveira, H. P. Facile Synthesis of Sustainable Biomass-Derived Porous Biochars as Promising Electrode Materials for High-Performance Supercapacitor Applications. *Nanomaterials* **2022**, *12*, 866.
(23) Huang, C.; Dong, Y.; Dong, X. Biomass based porous carbon for supercapacitor by hydrothermal assisted activating method. *E3S Web Conf.* **2021**, *236*, No. 01016.
(24) Kalu-Uka, G. M.; Kumar, S.; Kalu-Uka, A. C.; Vikram, S.; Ihekweme, G. O.; Ranjan, N.; Anosike-Francis, E. N.; Prajapati, G.; Nduba, A.; Onwualu, A. P.; Kumar, S. Production of Activated Carbon Electrode for Energy Storage Application in Supercapacitors via KOH Activation of Waste Termite Biomass. *Waste Biomass Valorization* **2022**, *13*, 2689−2704.
(25) Li, X.; Liu, K.; Liu, Z.; Wang, Z.; Li, B.; Zhang, D. Hierarchical porous carbon from hazardous waste oily sludge for all-solid-state flexible supercapacitor. *Electrochim. Acta* **2017**, *240*, 43−52.
(26) Mohamad Aziz, N. A.; Yunus, R.; Kania, D.; Abd Hamid, H. Prospects and Challenges of Microwave-Combined Technology for Biodiesel and Biolubricant Production through a Transesterification: A Review. *Molecules* **2021**, *26*, 788.
(27) Fuertes, A. B.; Ferrero, G. A.; Diez, N.; Sevilla, M. A Green Route to High-Surface Area Carbons by Chemical Activation of Biomass-Based Products with Sodium Thiosulfate. *ACS Sustain. Chem. Eng.* **2018**, *6*, 16323−16331.
(28) Ramasahayam, S. K.; Clark, A. L.; Hicks, Z.; Viswanathan, T. Spent coffee grounds derived P, N co-doped C as electrocatalyst for supercapacitor applications. *Electrochim. Acta* **2015**, *168*, 414−422.
(29) Shaku, B.; Mofokeng, T. P.; Coville, N. J.; Ozoemena, K. I.; Maubane-Nkadimeng, M. S. Biomass valorisation of marula nutshell waste into nitrogen-doped activated carbon for use in high performance supercapacitors. *Electrochim. Acta* **2023**, *442*, No. 141828.
(30) Yumak, T.; Yakaboylu, G. A.; Oginni, O.; Singh, K.; Ciftyurek, E.; Sabolsky, E. M. Comparison of the electrochemical properties of engineered switchgrass biomass-derived activated carbon-based EDLCs. *Colloids Surf. Physicochem. Eng. Asp.* **2020**, *586*, No. 124150.
(31) Wang, X.; Yun, S.; Fang, W.; Zhang, C.; Liang, X.; Lei, Z.; Liu, Z. Layer-Stacking Activated Carbon Derived from Sunflower Stalk as Electrode Materials for High-Performance Supercapacitors. *ACS Sustain. Chem. Eng.* **2018**, *6*, 11397−11407.
(32) Sevilla, M.; Diez, N.; Ferrero, G. A.; Fuertes, A. B. Sustainable supercapacitor electrodes produced by the activation of biomass with sodium thiosulfate. *Energy Storage Mater.* **2019**, *18*, 356−365.
(33) Mohamedkhair, A. K.; Aziz, Md.A.; Shah, S. S.; Shaikh, M. N.; Jamil, A. K.; Qasem, M. A. A.; Buliyaminu, I. A.; Yamani, Z. H. Effect of an activating agent on the physicochemical properties and supercapacitor performance of naturally nitrogen-enriched carbon derived from Albizia procera leaves. *Arab. J. Chem.* **2020**, *13*, 6161−6173.
(34) Tian, Z.; Li, J.; Zhu, G.; Lu, J.; Wang, Y.; Shi, Z.; Xu, C. Facile synthesis of highly conductive sulfur-doped reduced graphene oxide sheets. *Phys. Chem. Chem. Phys.* **2016**, *18*, 1125−1130.
(35) Mehdi, R.; Naqvi, S. R.; Khoja, A. H.; Hussain, R. Biomass derived activated carbon by chemical surface modification as a source of clean energy for supercapacitor application. *Fuel* **2023**, *348*, No. 128529.
(36) Men, B.; Guo, P.; Sun, Y.; Tang, Y.; Chen, Y.; Pan, J.; Wan, P. High-performance nitrogen-doped hierarchical porous carbon derived from cauliflower for advanced supercapacitors. *J. Mater. Sci.* **2019**, *54*, 2446−2457.
(37) Mu, J.; Li, Q.; Kong, X.; Wu, X.; Sunarso, J.; Zhao, Y.; Zhou, J.; Zhuo, S. Characterization of Hierarchical Porous Carbons Made from Bean Curd via K2CO3 Activation as a Supercapacitor Electrode. *ChemElectroChem.* **2019**, *6*, 4022−4030.
(38) Hayashi, J.; Horikawa, T.; Takeda, I.; Muroyama, K.; Nasir Ani, F. Preparing activated carbon from various nutshells by chemical activation with K2CO3. *Carbon* **2002**, *40*, 2381−2386, DOI: 10.1016/S0008-6223(02)00118-5.
(39) Kim, E.-K.; Lee, B.-M.; Park, J.-J.; Choi, J.-H.; Yun, J. M. Hierarchically porous carbon materials synthesized from sustainable tannic acid with sodium citrate via ice-templating and carbonization for high-performance supercapacitors. *Mater. Today Sustain.* **2022**, *20*, No. 100238.
(40) Pang, J.; Zhang, W.; Zhang, J.; Cao, G.; Han, M.; Yang, Y. Facile and sustainable synthesis of sodium lignosulfonate derived hierarchical porous carbons for supercapacitors with high volumetric energy densities. *Green Chem.* **2017**, *19*, 3916−3926.
(41) Zhang, J.; Zhang, W.; Han, M.; Pang, J. One pot synthesis of nitrogen-doped hierarchical porous carbon derived from phenolic

https://doi.org/10.1021/acsomega.3c09438
ACS Omega 2024, 9, 13134−13147

formaldehyde resin with sodium citrate as activation agent for supercapacitors. *J. Mater. Sci. Mater. Electron.* **2018**, *29*, 4639−4648.
(42) Vijayakumar, M.; Bharathi Sankar, A.; Sri Rohita, D.; Rao, T. N.; Karthik, M. Conversion of Biomass Waste into High Performance Supercapacitor Electrodes for Real-Time Supercapacitor Applications, ACS Sustain. *Chem. Eng.* **2019**, *7*, 17175−17185.
(43) Lu, Y.; Zhang, S.; Yin, J.; Bai, C.; Zhang, J.; Li, Y.; Yang, Y.; Ge, Z.; Zhang, M.; Wei, L.; Ma, M.; Ma, Y.; Chen, Y. Data on high performance supercapacitors based on mesoporous activated carbon materials with ultrahigh mesopore volume and effective specific surface area. *Data Brief* **2018**, *18*, 1448−1456.
(44) Chen, R.; Tang, H.; He, P.; Zhang, W.; Dai, Y.; Zong, W.; Guo, F.; He, G.; Wang, X. Interface Engineering of Biomass-Derived Carbon used as Ultrahigh-Energy-Density and Practical Mass-Loading Supercapacitor Electrodes. *Adv. Funct. Mater.* **2023**, *33*, 2212078.
(45) Dyatkin, B.; Presser, V.; Heon, M.; Lukatskaya, M. R.; Beidaghi, M.; Gogotsi, Y. Development of a green supercapacitor composed entirely of environmentally friendly materials. *ChemSusChem* **2013**, *6*, 2269−2280.
(46) Liu, J.; Wang, J.; Xu, C.; Jiang, H.; Li, C.; Zhang, L.; Lin, J.; Shen, Z. X. Advanced Energy Storage Devices: Basic Principles, Analytical Methods, and Rational Materials Design. *Adv. Sci.* **2018**, *5*, 1700322.
(47) Jain, A.; Xu, C.; Jayaraman, S.; Balasubramanian, R.; Lee, J. Y.; Srinivasan, M. P. Mesoporous activated carbons with enhanced porosity by optimal hydrothermal pre-treatment of biomass for supercapacitor applications. *Microporous Mesoporous Mater.* **2015**, *218*, 55−61.
(48) Qu, W.-H.; Xu, Y.-Y.; Lu, A.-H.; Zhang, X.-Q.; Li, W.-C. Converting biowaste corncob residue into high value added porous carbon for supercapacitor electrodes. *Bioresour. Technol.* **2015**, *189*, 285−291.
(49) Sun, F.; Gao, J.; Liu, X.; Pi, X.; Yang, Y.; Wu, S. Porous carbon with a large surface area and an ultrahigh carbon purity via templating carbonization coupling with KOH activation as excellent supercapacitor electrode materials. *Appl. Surf. Sci.* **2016**, *387*, 857−863.
(50) Qian, W.; Sun, F.; Xu, Y.; Qiu, L.; Liu, C.; Wang, S.; Yan, F. Human hair-derived carbon flakes for electrochemical supercapacitors. *Energy Environ. Sci.* **2014**, *7*, 379−386.
(51) Wu, L.; Cai, Y.; Wang, S.; Li, Z. Doping of nitrogen into biomass-derived porous carbon with large surface area using N2 non-thermal plasma technique for high-performance supercapacitor. *Int. J. Hydrog. Energy* **2021**, *46*, 2432−2444.
(52) Liu, W.; Mei, J.; Liu, G.; Kou, Q.; Yi, T.; Xiao, S. Nitrogen-Doped Hierarchical Porous Carbon from Wheat Straw for Supercapacitors. *ACS Sustain. Chem. Eng.* **2018**, *6*, 11595−11605.
(53) Xia, J.; Zhang, N.; Chong, S.; Li, D.; Chen, Y.; Sun, C. Three-dimensional porous graphene-like sheets synthesized from biocarbon via low-temperature graphitization for a supercapacitor. *Green Chem.* **2018**, *20*, 694−700.
(54) Lobato-Peralta, D. R.; Amaro, R.; Arias, D. M.; Cuentas-Gallegos, A. K.; Jaramillo-Quintero, O. A.; Sebastian, P. J.; Okoye, P. U. Activated carbon from wasp hive for aqueous electrolyte supercapacitor application. *J. Electroanal. Chem.* **2021**, *901*, No. 115777.
(55) Liu, S.; Zhao, Y.; Zhang, B.; Xia, H.; Zhou, J.; Xie, W.; Li, H. Nano-micro carbon spheres anchored on porous carbon derived from dual-biomass as high rate performance supercapacitor electrodes. *J. Power Sources* **2018**, *381*, 116−126.

https://doi.org/10.1021/acsomega.3c09438
ACS Omega 2024, 9, 13134−13147